Probing the evolution of Stark wave packets by a weak half-cycle pulse

H. Wen, S. N. Pisharody, J. M. Murray, and P. H. Bucksbaum

FOCUS Center, Department of Physics, University of Michigan, Ann Arbor, Michigan 48109-1120, USA

(Received 14 July 2004; published 12 January 2005)

We probe the dynamic evolution of a Stark wave packet in cesium using weak half-cycle pulses (HCP's). The state-selective field-ionization spectra taken as a function of HCP delay reveal wave-packet dynamics such as Kepler beats, Stark revivals, and fractional revivals. A quantum-mechanical simulation explains the results as multimode interference induced by the HCP.

I. INTRODUCTION

Recent publications have shown that Rydberg states in an atom can be used as data storage registers for quantum information processing [1]. A significant limitation is that relatively few states couple directly to the atomic ground state via allowed transitions, so that the full range of Rydberg state quantum numbers cannot participate in quantum information operations. Quantum control methods have been proposed to extend the data registers to include angular momentum states [2]. To utilize this approach for information storage, the angular momentum content of high-ℓ Rydberg wave packets must be measured with reasonable fidelity. Here, we show how to approach this using electromagnetic half-cycle pulses (HCP's) and state-selective field ionization (SSFI).

Several experiments have utilized correspondence between classical and quantum systems to relate classical dynamics to the control and manipulation of a quantum system [3–5]. Meanwhile, other experiments have utilized a direct quantum-mechanical approach to understand and control the quantum properties of the wave packets [6–8]. In either the classical or the quantum-mechanical context, the efficient detection of a wave packet is always a challenge. Several detection methods have been used with varying degrees of success, for example, short pulse pump-probe ionization [9], bound-state interferometry [10], and time-resolved streak camera detection of ionization [11]. Detection of Stark wave-packet dynamics has also been demonstrated using HCP's [12–14]. In those previous experiments, the detection relies on the fact that an HCP induces a change of an electron's total energy, $\Delta E = \vec{p} \cdot \vec{Q} + \vec{Q}^2/2$, to ionize the electrons. Here, $\vec{Q}$ represents the momentum transferred to electrons from the HCP and $\vec{p}$ is the initial momentum of the electron. In these experiments, the ionization of the atoms by HCP-assisted transfer of momentum to the electrons is used to retrieve the classical dynamics of the electronic wave packet. However, these methods of detection are insensitive to the effect of the HCP on the bound-state population distribution in the wave packet. In the context of quantum information processing, control over the amplitudes and phases of each of the states in the wave packet is essential for the manipulation of quantum information.

In this work, we use a weak HCP to probe the evolution of a Stark wave packet. The population redistribution in the wave packet due to the HCP [15] is detected by SSFI. Kepler beats, angular momentum revivals, and fractional revivals are all clearly observed in the HCP-delay-dependent SSFI spectra. In contrast to time-delay spectroscopy [16] and impulsive momentum retrieval [17], the strength of the HCP's used in this experiment are much smaller than that required to directly ionize the atoms.

II. EXPERIMENTAL PROCEDURE

A thermal beam of cesium atoms in a uniform electric field, $F\hat{z}$, are driven from the $6s$ ground state to the $7s$ launch state via two-photon excitation by the focused 1079-nm output of a Ti:sapphire-laser-pumped optical parametric amplifier. A shaped, amplified, ultrafast laser pulse excites Stark wave packets with $m_\ell=0$ in the range of $24 \leqslant n^* \leqslant 28$.

A weak HCP with a peak field of about 1 kV/cm and a pulse width of 400 fs is applied along the direction of the static electric field following the creation of the Stark wave packet. The HCP is created by illuminating a high-voltage-biased GaAs photoconductive switch with the 800-nm, 50-fs output of the Ti:Sapphire laser. The HCP applies an impulse of 0.002 a.u. (atomic units: $e=m_e=\hbar=1$) to the electrons. This redistributes the bound-state populations and produces multimode interference depending on the relative phases of the states. About 10 μs after this impulse, SSFI is used to detect the energy-level composition of the wave packet.

In the absence of an HCP, SSFI is insensitive to the evolution of the angular momentum composition of the states in the wave packet. A weak HCP differentiates the SSFI spectra based on the time-dependent angular momentum composition of the wave packet. We can then use the SSFI spectra of the HCP-kicked Stark wave packet to calibrate its angular momentum composition.

III. DATA ANALYSIS

A wave packet excited from the 7-s launch state in Cs to a set of excited Rydberg states in the presence of an external electric field has p-state character immediately after its excitation. Angular momentum, however, is not a good quantum number for Rydberg states in an electric field. The coupling of angular momentum in the different energy levels of the Stark wave packet results in the time-dependent variation of the angular momentum of the wave packet [2]. This is shown
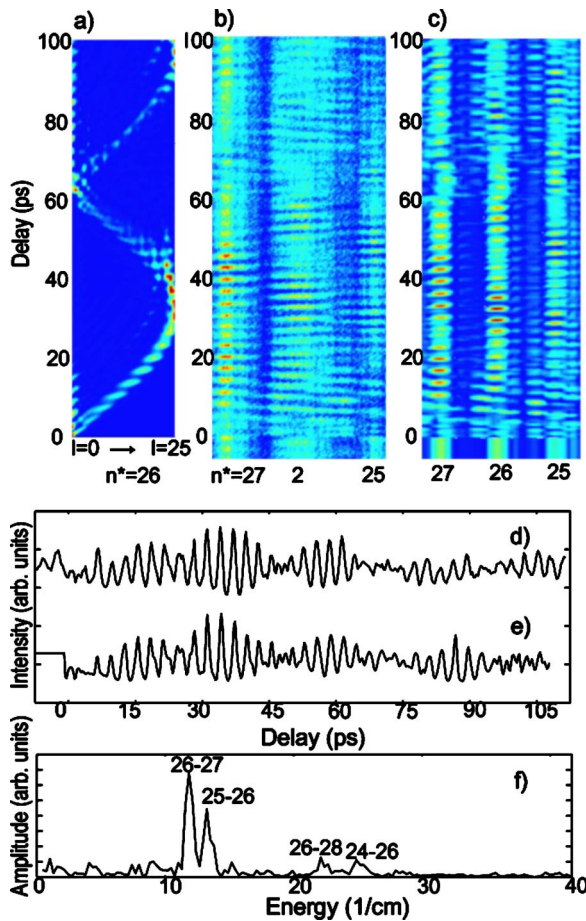
FIG. 1. (Color online) (a) The angular momentum components of the $n^* \sim 26$ state in the Stark wave packet as a function of time following wave-packet excitation; (b) The state-resolved, HCP-induced, time-dependent spectrum, known as a quantum carpet. The ionization signal (color) of four manifolds ($25 \leqslant n^* \leqslant 28$) is shown as a function of HCP delay in a static electric field $F = 160$ V/cm; (c) the calculated quantum carpet for (b); (d) the ionization signal for $n^* \sim 26$ as a function of HCP delay; (e) the calculated ionization signal for (d); (f) the Fourier transform of (d).

FIG. 2. The Stark energy levels for Cs ($m=0$) in the range of $24 \leqslant n^* \leqslant 28$. The darkness of the lines indicates the photoexcitation probability at the applied external electric fields.

in Fig. 1(a). In the presence of the static electric field, the angular momentum of the n manifold in the Stark wave packet precesses from low ℓ to high ℓ and back over the course of a Stark period of $\sim 2\pi/3Fn$. The angular momentum evolution is understood classically as a precession of the electron orbit under the influence of the external electric field.

Figure 1(b) shows the SSFI spectrum plotted as a function of the delay of the HCP kick relative to the creation of the Stark wave packet for the case of an external electric field of 160 V/cm. The HCP redistributes the population in the different manifolds depending on the instantaneous angular momentum composition and phase of the states in the wave packet. The spectrum at the bottom of the graph (for delay $\leqslant 0$) corresponds to the initial population distribution in the Stark wave packet before the HCP interaction (Fig. 2). For the first 10–15 ps following the excitation of the wave packet, the HCP redistributes population predominantly into low angular momentum states. The SSFI spectrum changes
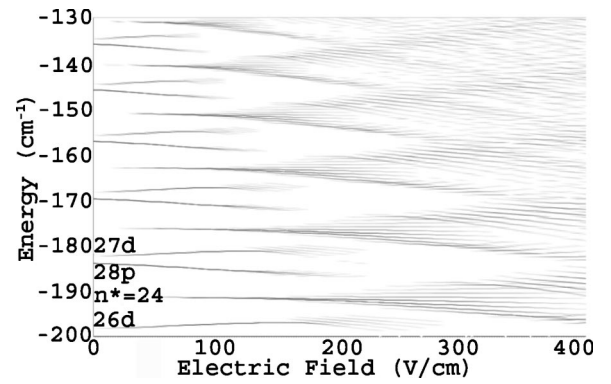
significantly in this regime due to the large quantum defects for the p and d states compared to the other states in the manifold. At later delays of the HCP, there are periodic modulations in intensity of the SSFI spectrum for each of the states in the wave packet. A lineout of the intensity variation in the spectrum corresponding to the $n^* \sim 26$ state is shown in Fig. 1(d). We find that the spectrum returns to its low angular momentum form at HCP delays around 64 ps. This corresponds to the Stark period ($2\pi/3Fn$) of a wave packet centered around $n^* \sim 26$ at a field of 160 V/cm. The envelope of intensity modulations over one Stark period also displays minima in intensity at times 26 and 48 ps. This temporal structure corresponds to the fractional revival periods, $\tau_f = 2\pi n^4/3$ [18]. Around these visibility minima, the Kepler beats double in frequency [19] due to a splitting of the wave packet into two parts.

The Fourier transform of Fig. 1(d) is shown in Fig. 1(f). The peaks correspond to the energy differences between the state $n^* \sim 26$ and its neighboring states. The weak HCP acts to couple neighboring n states and to produce interference between different n manifolds in the Stark wave packet. The two strongest frequency components are attributed to the energy differences of its neighboring states $\Delta E_{26,27} = 11.8$ cm^{-1} and $\Delta E_{25,26} = 13.3$ cm^{-1}. The two weaker peaks correspond to the energy differences of its next-neighbor states $\Delta E_{26,28} = 22.4$ cm^{-1} and $\Delta E_{24,26} = 24.8$ cm^{-1}. The deviation of $\Delta E_{24,26}$ from the zero-field value of 28.2 cm^{-1} is due to manifold mixing at $F = 160$ V/cm so that the HCP couples the Stark states at the edge of the $n^* \sim 26$ manifold instead of in the middle.

At low electric fields, the p and d states are completely separated in energy from the higher angular momentum components of the Stark manifolds. The pattern for $F = 80$ V/cm in Fig. 3(a) shows dominant population shifts from low-energy states to high-energy states as a function of the HCP delay. This "quantum carpet" pattern fits well with the Kepler periods for corresponding n states in the wave packet [7]. The dark lines in the figure are plotted to represent the expected times for Kepler revivals ($\tau_{Kepler} = 2\pi n^3$) for each state in the wave packet. These are found to correspond very closely to the observed maxima in the HCP-assisted population redistribution in the wave packet. In Fig.
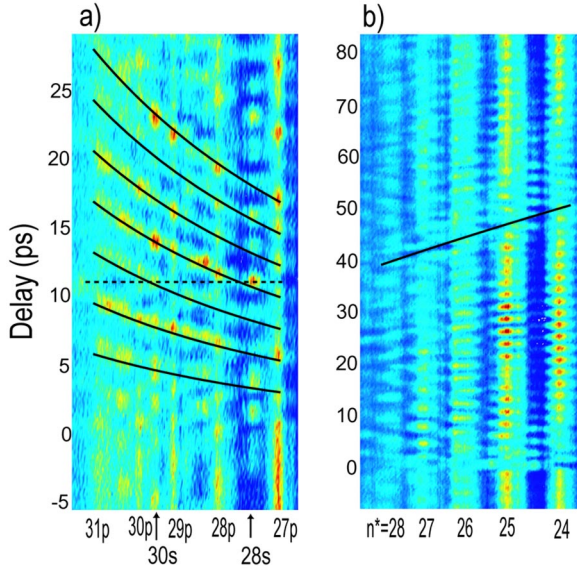
FIG. 3. (Color online) (a) The quantum carpet for F $=80$ V/cm. The dark lines represent the successive energy-dependent Kepler periods ($\tau_{Kepler}=2\pi n^3$); (b) The quantum carpet for $F=240$ V/cm. The dark line represents the Stark revival time $\tau_{Stark}=2\pi/3Fn$.

3(b), where $F=240$ V/cm, a calculated line indicates the expected times for angular momentum revivals (τ_{Stark} $=2\pi/3Fn$). This matches the repetition of the extended features in the SSFI spectrum seen in the experiment.

Figure 3(a) also demonstrates the use of a weak HCP to selectively populate particular low angular momentum states by an intelligent choice of HCP delay. The HCP arriving at the interaction region 11 ps after the creation of the Stark wave packet in an external field of 80 V/cm selectively populates the 28s and the 30s states while removing population from the other states.

IV. NUMERICAL SIMULATION

We have performed numerical simulations to gain further insight into our experimental results. We model the HCP [$\vec{\mathcal{F}}(t)$] as an impulsive momentum kick to the electronic Stark wave packet [8].

The interaction Hamiltonian of the HCP is written as

$$H(t) = \vec{\mathcal{F}}(t) \cdot \vec{r}, \tag{1}$$

where we have used atomic units throughout. The result of the HCP interaction with the wave packet can then be written as

$$|\Psi_f(t)\rangle = e^{i\vec{Q}\cdot\vec{r}}|\Psi_i(t)\rangle, \tag{2}$$

where $|\Psi_{i,f}(t)\rangle$ are the wave packets in the basis of the Stark Hamiltonian before and after the interaction with the HCP. The integral $\vec{Q}=-\int\vec{\mathcal{F}}(t')dt'$ represents the total momentum transferred to the electron. The $\hat{z}$-polarized HCP is modeled as a unitary operator e^{iQz} in the impulse approximation. Immediately before the arrival of the HCP, Ψ is written as

$$|\Psi_i(t)\rangle = \sum_{nk} c_{nk}e^{-i\omega_{nk}t}|nk\rangle. \tag{3}$$

After the interaction with the HCP, the Ψ becomes

$$|\Psi_f(t)\rangle = e^{iQz}|\Psi_i(t)\rangle = \sum_{nk,n'k'} \mathcal{M}_{n'k',nk}c_{nk}e^{-i\omega_{nk}t}|n'k'\rangle, \tag{4}$$

where

$$\mathcal{M}_{n'k',nk} = \langle n'k'|e^{iQz}|nk\rangle \tag{5}$$

represents the HCP effect. The coupling matrix elements are calculated in the field-free $n\ell m$ basis and subsequently transformed into the nkm (Stark) basis using the transformation matrix that diagonalizes the Stark Hamiltonian, $H=(p^2/2)$ $-1/r+Fz$. The strongest HCP coupling occurs between the states in adjacent manifolds rather than between states within the same manifold. For the HCP strengths used, the dominant coupling occurs for states separated by one or two manifolds. This explains the observed energy-level contributions to the dynamics in Fig. 1(e). Multimode interference due to HCP coupling among neighboring manifolds enhances the Kepler-period modulations in the observed SSFI spectra.

The calculations are performed over a range of energies corresponding to $10 \leq n^* \leq 40$. The state distribution in the final wave packet after the HCP interaction is mapped from its energy, E, to the expected ionization field, ($F_i=E^2/4$), for comparison to the experimental SSFI spectrum. The results of our simulations with an external electric field of 160 V/cm is shown in Fig. 1(c) and the lineout corresponding to the $n^* \sim 26$ state is shown in Fig. 1(e). The results of our simulations are in excellent agreement with the experiment.

V. DISCUSSION AND CONCLUSIONS

An HCP acting on an electronic wave packet changes the electron energy depending on its instantaneous linear momentum along the direction of the HCP. This feature has enabled experiments in the past that have used directed HCP's to map the time-resolved momentum distribution of the electron in its orbit [13,14]. When the Stark wave packet evolves to high angular momentum, the corresponding classical orbits of the electron are along the lines of constant longitude on the surface of a sphere where the poles are aligned in the direction of the electric field. In the semiclassical picture, the high angular momentum $m=0$ electron wave packet is well localized radially and oscillates in latitude between the poles [14]. Such a wave packet has a linear momentum aligned along the electric field at times separated by a Kepler period when it is localized at angles corresponding to the equator on the sphere. The wave packet also has the least linear momentum in the direction of the HCP at times when it is localized close to the poles of the sphere. This maximal variation in linear momentum character and therefore maximal variation in energy transfer to the electrons can be seen in our data and simulations to correspond to the greatest contrast in Figs. 1(d) and 1(e) at times around 33 ps.

In summary, we employ a weak HCP as a coherent redistribution operator to probe the Stark wave packet. The quantum carpet that we obtain reveals three characteristic times: the Kepler beats, the Stark revivals, and the fractional revivals, and agrees well with their expected n dependence. Our simulations using an impulse model for the HCP are in excellent agreement with the experimental results. The use of a weak HCP to differentiate the instantaneous angular momentum composition of a Stark wave packet could, in the future, allow us to use SSFI as a single-shot detector for angular momentum states.

[1] J. Ahn, T. C. Weinacht, and P. H. Bucksbaum, Science **287**, 463 (2000).

[2] H. Wen, C. Rangan, and P. H. Bucksbaum, Phys. Rev. A **68**, 053405 (2003).

[3] J. Bromage and C. R. Stroud, Jr., Phys. Rev. Lett. **83**, 4963 (1999).

[4] D. G. Arbo, C. O. Reinhold, J. Burgdrfer, A. K. Pattanayak, C. L. Stokely, W. Zhao, J. C. Lancaster, and F. B. Dunning, Phys. Rev. A **67**, 063401 (2003).

[5] C. L. Stokely, F. B. Dunning, C. O. Reinhold, and A. K. Pattanayak, Phys. Rev. A **65**, 021405 (1996).

[6] T. C. Weinacht, J. Ahn, and P. H. Bucksbaum, Phys. Rev. Lett. **80**, 5508 (1998).

[7] J. Ahn, D. N. Hutchinson, C. Rangan, and P. H. Bucksbaum, Phys. Rev. Lett. **86**, 1179 (2001).

[8] J. Ahn, C. Rangan, D. N. Hutchinson, and P. H. Bucksbaum, Phys. Rev. A **66**, 022312 (2002).

[9] L. D. Noordam, A. ten Wolde, A. Lagendijk, and H. B. van Linden van den Heuvell, Phys. Rev. A **40**, 6999 (1989).

[10] M. L. Naudeau, C. I. Sukenik, and P. H. Bucksbaum, Phys. Rev. A **56**, 636 (1997).

[11] G. M. Lankhuijzen and L. D. Noordam, Phys. Rev. Lett. **76**, 1784 (1996).

[12] M. B. Campbell, T. J. Bensky, and R. R. Jones, Phys. Rev. A **58**, 514 (1998).

[13] M. B. Campbell, T. J. Bensky, and R. R. Jones, Phys. Rev. A **59**, R4117 (1999).

[14] C. S. Raman, T. C. Weinacht, and P. H. Bucksbaum, Phys. Rev. A **55**, R3995 (1997).

[15] N. E. Tielking and R. R. Jones, Phys. Rev. A **52**, 1371 (1995).

[16] C. Raman, C. W. S. Conover, C. I. Sukenik, and P. H. Bucksbaum, Phys. Rev. Lett. **76**, 2436 (1996).

[17] R. R. Jones, Phys. Rev. Lett. **76**, 3927 (1996).

[18] J. A. Yeazell, M. Mallalieu, and C. R. Stroud, Jr., Phys. Rev. Lett. **64**, 2007 (1990).

[19] J. A. Yeazell and C. R. Stroud, Jr., Phys. Rev. A **43**, 5153 (1991).